ELEKTROTEHNIŠKI VESTNIK 81(1-2): 57-63, 2014
ORIGINAL SCIENTIFIC PAPER

Fault-Current Study of the Wind-Turbine-Driven Doubly-Fed Induction Generator with the Crowbar Protection

Xiangping Kong, Zhe Zhang

State Key Laboratory of Advanced Electromagnetic Engineering and Technology (Huazhong University of Science and Technology), Wuhan 430074, Hubei, China
Email: kongxphust@163.com

Abstract. The crowbar protection is commonly used for wind turbines with a doubly-fed induction generator (DFIG) to enhance the low-voltage ride-through capability of the wind turbines. Thus, the fault-current characteristics of DFIG with the crowbar protection under symmetric- and asymmetric-fault states are studied in this paper. Firstly, a DFIG dynamic model in the stator stationary reference frame is developed and the dynamic characteristics of DFIG stator flux linkage are studied when the crowbar protection is activated. Based on it, the DFIG fault-current characteristics under symmetric- and asymmetric-fault states are analyzed and analytical expressions are obtained. Finally, the simulation results show that the accuracy of the theoretical analysis results is satisfactory to meet the requirements of the study of the relay-protection principle and calculation.

Keywords: doubly-fed induction generator (DFIG), crowbar protection, stator flux linkage, fault-current characteristics

Zaščita delovanja vetrnih elektrarn z dvojno napajanim asinhronskim generatorjem ob kratkostičnih motnjah

Najpogostejši način zaščite vetrnih elektrarn z dvojno napajanim asinhronskim generatorjem ob kratkostičnih motnjah v sistemu je zaščita pretvornika v rotorskem tokokrogu s premostitvenim uporom in polprevodniškim stikalom (angl. crowbar). V članku analiziramo kratkostično tokovno karakteristiko vetrnih elektrarn ob simetričnih in nesimetričnih motnjah. V ta namen najprej razvijemo dinamični model dvojno napajanega asinhronskega generatorja v statorskem referenčnem koordinatnem sistemu, na podlagi katerega analiziramo dinamično obnašanje statorskih magnetnih sklepov ob aktivaciji zaščite. Nato razvijemo ustrezne analitične izraze, ki služijo podrobni analizi obnašanja vetrnih elektrarn ob simetričnih in nesimetričnih motnjah v sistemu. Na koncu podamo še simulacijske rezultate, ki kažejo ustrezno obnašanje in zadostujejo kriterijem nastavitve zaščit.

1 INTRODUCTION

Recently, as the most commercialized one of the renewable energy sources, the wind-power generation has been developed greatly all over the world. The most common type of the wind turbine which has been widely applied is the doubly-fed induction generator (DFIG), since it has the advantages of a small capacity of the converter, high energy-conversion efficiency and flexible power control [1-3]. DFIG comprises a wound-rotor induction generator with its stator windings connected to the power grid directly and rotor windings interfaced to the power grid with an AC/DC/AC converter. The AC/DC/AC converter consists of a rotor-side converter (RSC) and a grid-side converter (GSC) connected back-to-back by a dc-link capacitor.

However, with the increasing grid-connected wind-power capacity, in order to ensure safe operation of the power gird and wind turbines, the power system operators have issued new grid codes to require the wind turbines to have the low-voltage ride-through (LVRT) capability [4]-[6].

In order to enhance the LVRT capability and ensure safe DFIG operation during a grid fault, one commonly used approach is to install the crowbar protection [7]. When the power-grid fault makes the rotor current too large or the dc-link voltage too high, the crowbar protection is activated to short-circuit the rotor windings with the crowbar resistance and divert the current from RSC. Activation of the crowbar protection causes the loss of the excitation current and consequently makes DFIG change from the generator to the motor. Meanwhile, introduction of the crowbar resistance makes the coupling between the stator and the rotor windings increase significantly. Hence, the DFIG operating characteristics are much different not only from those of the synchronous generator, but also from those of the induction motor.

Moreover, the DFIG operating characteristics under the LVRT state considerably affect the characteristics of the fault voltage and fault current, which causes many

Received 9 January 2014
Accepted 27 February 2014

new challenges to the traditional relay protection of the power grid [8]. Hence, in order to address the relay protection issues and ensure the safe operation of the power grid with DFIGs, the operating and the fault-current characteristics of DFIG under the LVRT state should be studied.

So far, many scholars have carried out research works to study the DFIG fault-current characteristics under the three-phase short-circuit state [9-13]. However, the existing research results are either qualitative or obtained by the analogy with the fault-current characteristics of the conventional synchronous generator or induction motor. It means that the DFIG inherent features when the crowbar protection is activated are not taken into account. Furthermore, there is little literature discussing the DFIG fault-current characteristics under asymmetric-fault states. However, the possibility of the asymmetric-faults occurrence is much larger than the symmetric faults. The study of the DFIG fault-current characteristics under the asymmetric-fault states is the important part of the comprehensive analysis of the DFIG fault-current characteristics.

In order to fill the gap, the DFIG fault current under the states of the symmetric and asymmetric faults is analyzed in this paper. During a grid fault, the fault current provided by DFIG consists of the stator-side fault current and the grid-side fault current of GSC. However, the fault current provided by GSC is very small, since the capacity of GSC is only 25-30% of the rated capacity of the wind turbine. Hence, only the stator fault current is taken into account in this paper.

In Section II, a dynamic model of DFIG in the stator stationary reference frame is developed. In Section III, the dynamic characteristics of the stator flux linkage of DFIG are studied when the crowbar protection is activated and a simplified calculation model of the stator flux linkage is built. Then the DFIG fault-current characteristics under the states of symmetric and asymmetric faults are analyzed and the analytical expressions are obtained in Section IV. Finally, the simulation cases are studied in Section V to validate the theoretical analysis results.

2 DFIG DYNAMIC MODEL

The generalized voltage and flux-linkage equations of DFIG are expressed in (1) and (2). It is noted that the motor convention is adopted both for the stator and rotor windings.

$$\begin{pmatrix} \boldsymbol{U}_s \\ \boldsymbol{U}_r \end{pmatrix} = \begin{pmatrix} \boldsymbol{R}_s & 0 \\ 0 & \boldsymbol{R}_r \end{pmatrix} \begin{pmatrix} \boldsymbol{I}_s \\ \boldsymbol{I}_r \end{pmatrix} + \frac{d}{dt} \begin{pmatrix} \boldsymbol{\Psi}_s \\ \boldsymbol{\Psi}_r \end{pmatrix} \tag{1}$$

$$\begin{pmatrix} \boldsymbol{\Psi}_s \\ \boldsymbol{\Psi}_r \end{pmatrix} = \begin{pmatrix} \boldsymbol{L}_s & \boldsymbol{L}_{sr} \\ \boldsymbol{L}_{sr}^T & \boldsymbol{L}_r \end{pmatrix} \begin{pmatrix} \boldsymbol{I}_s \\ \boldsymbol{I}_r \end{pmatrix} \tag{2}$$

where $\boldsymbol{U}_s$, $\boldsymbol{U}_r$, $\boldsymbol{I}_s$, $\boldsymbol{I}_r$, $\boldsymbol{\Psi}_s$ and $\boldsymbol{\Psi}_r$ are the matrices of the voltage, current and flux linkage respectively of the stator and rotor windings.

Since the mutual inductance matrix between the stator and rotor windings is time-varying, it is difficult to be solved. The method commonly used in the existing literatures is to perform a synchronous (i.e. dq) coordinate transformation to (1) and (2). However, in this context, both the reference frame rotating at a positive synchronous speed and the reference frame rotating at a negative synchronous speed are needed under the asymmetric-fault states [14]. Meanwhile, the positive- and the negative-sequence components should be extracted. Hence, when an asymmetric-fault occurs, implementation of dq coordinate transformation would result in a severe complexity to the fault-current study of DFIG.

Since the structure and electromagnetic property of the DFIG rotor windings are symmetrical, the stator stationary reference frame should be adopted for coordinate transformation to simplify the analysis.

Under the stator stationary (i.e. $\alpha\beta$) reference frame, the DFIG voltage and flux-linkage equations are given in (3) and (4).

$$\begin{bmatrix} u_{s\alpha} \\ u_{s\beta} \\ u_{r\alpha} \\ u_{r\beta} \end{bmatrix} = \begin{bmatrix} R_s & & & \\ & R_s & & \\ & & R_r & \\ & & & R_r \end{bmatrix} \begin{bmatrix} i_{s\alpha} \\ i_{s\beta} \\ i_{r\alpha} \\ i_{r\beta} \end{bmatrix} + \begin{bmatrix} d\psi_{s\alpha}/dt \\ d\psi_{s\beta}/dt \\ d\psi_{r\alpha}/dt + \omega_r \psi_{r\beta} \\ d\psi_{r\beta}/dt - \omega_r \psi_{r\alpha} \end{bmatrix} \tag{3}$$

$$\begin{bmatrix} \psi_{s\alpha} \\ \psi_{s\beta} \\ \psi_{r\alpha} \\ \psi_{r\beta} \end{bmatrix} = \begin{bmatrix} L_s & & L_m & \\ & L_s & & L_m \\ L_m & & L_r & \\ & L_m & & L_r \end{bmatrix} \begin{bmatrix} i_{s\alpha} \\ i_{s\beta} \\ i_{r\alpha} \\ i_{r\beta} \end{bmatrix} \tag{4}$$

where $\omega_r = (1-s)\omega_1$, representing the rotor angular speed; s is the slip and ω_1 is the synchronous angular frequency.

Taking the stator flux linkage and rotor flux linkage as the state variables, the DFIG state equations are given by

$$\frac{d}{dt} \begin{bmatrix} \psi_{s\alpha} \\ \psi_{s\beta} \\ \psi_{r\alpha} \\ \psi_{r\beta} \end{bmatrix} = \mathbf{A} \begin{bmatrix} \psi_{s\alpha} \\ \psi_{s\beta} \\ \psi_{r\alpha} \\ \psi_{r\beta} \end{bmatrix} + \begin{bmatrix} u_{s\alpha} \\ u_{s\beta} \\ u_{r\alpha} \\ u_{r\beta} \end{bmatrix} \tag{5}$$

$$\begin{bmatrix} i_{s\alpha} \\ i_{s\beta} \\ i_{r\alpha} \\ i_{r\beta} \end{bmatrix} = \frac{1}{L_t} \begin{bmatrix} L_r & & -L_m & \\ & L_r & & -L_m \\ -L_m & & L_s & \\ & -L_m & & L_s \end{bmatrix} \begin{bmatrix} \psi_{s\alpha} \\ \psi_{s\beta} \\ \psi_{r\alpha} \\ \psi_{r\beta} \end{bmatrix} \tag{6}$$

where $L_t = L_s L_r - L_m^2$,

$$\boldsymbol{A}=\left[\begin{array}{cc:cc} -R_sL_r/L_t & & R_sL_m/L_t & \\ & -R_sL_r/L_t & & R_sL_m/L_t \\ \hdashline R_rL_m/L_t & & -R_rL_s/L_t & -\omega_r \\ & R_rL_m/L_t & \omega_r & -R_rL_s/L_t \end{array}\right].$$

As it is known, the damping time constants and oscillation frequencies of the stator flux- linkage and rotor flux linkage are determined by the eigenvalues of the system matrix $\boldsymbol{A}$. Meanwhile, the damping time constants and oscillation frequencies of the transient components of the stator- and rotor-fault currents are also determined by the eigenvalues of the system matrix $\boldsymbol{A}$.

3 STUDY OF THE STATOR FLUX LINKAGE

3.1 Characteristics analysis of the stator flux linkage

In matrix $\boldsymbol{A}$, the terms R_sL_m/L_t and R_rL_m/L_t indicate the coupling between the stator flux linkage and rotor flux linkage. Under a normal operating state, since both the stator and rotor resistances are small, R_sL_m/L_t and R_rL_m/L_t are also very small. It means that the coupling between the stator flux linkage and rotor flux linkage can be neglected under a normal operating state. Hence, the matrix $\boldsymbol{A}$ can be rewritten as

$$\boldsymbol{A}=\left[\begin{array}{cc:cc} -R_sL_r/L_t & & & \\ & -R_sL_r/L_t & & \\ \hdashline & & -R_rL_s/L_t & -\omega_r \\ & & \omega_r & -R_rL_s/L_t \end{array}\right] \quad (7)$$

The eigenvalues of the matrix $\boldsymbol{A}$ are given by

$$\begin{cases} p_{1,2}=-1/\tau_{As}\pm j\omega_{As}=-R_sL_r/L_t \\ p_{3,4}=-1/\tau_{Ar}\pm j\omega_{Ar}=-R_rL_s/L_t\pm j\omega_r \end{cases} \quad (8)$$

where τ_{As} is the damping time constant of the transient components of the stator flux linkage, τ_{Ar} is the damping time constant of the transient components of the rotor flux linkage, τ_{As} is the damping time constant of the transient components of the stator flux linkage and ω_{Ar} is the oscillation frequency of the transient components of the rotor flux linkage.

In this context, the stator flux linkage and rotor flux linkage can be studied according to two independent second-order systems.

If a severe fault occurs near DFIG, the crowbar protection is activated to ensure safe DFIG operation. By introducing the crowbar resistance, the equivalent resistance of the rotor windings R_r' is

$$R_r'=R_r+R_c \quad (9)$$

where R_c is the crowbar resistance.

This makes the coupling between the stator flux linkage and rotor flux linkage increase significantly, which can no longer be neglected. Hence, the research results of the DFIG fault current based on the simplification that the impact of the stator and rotor resistances can be neglected [9] or by the analogy with the fault-current characteristics of the induction motor [10,11] cannot agree with the reality very well.

Replacing R_r in (7) with R_r', a new system matrix $\boldsymbol{A}_c$ after activation of the crowbar protection can be obtained. The corresponding eigenvalues are expressed in (10).

$$p_{c1,2}=-1/\tau_{Acs}\pm j\omega_{Acs}\ ,\ \ p_{c3,4}=-1/\tau_{Acr}\pm j\omega_{Acr} \quad (10)$$

Specifically for 1.5 MW-rated DFIG (the detailed parameters are given in Appendix A), Table 1 shows the impact of the crowbar resistance on the eigenvalues of matrix $\boldsymbol{A}_c$.

As seen from Table 1, though the crowbar resistance affects both the real and the imaginary parts of the eigenvalues of matrix $\boldsymbol{A}_c$, the impact of the crowbar resistance on the imaginary part (i.e. oscillation frequencies of the transient components) is rather small. The maximum value of ω_{Acs} is 3.68rad/s and the minimum value of ω_{Acr} is 373.31 rad/s, hence, it can be approximately considered that

$$\omega_{Acs}\approx 0\ ,\ \omega_{Acr}\approx\omega_r \quad (11)$$

i.e., there are only an ac component with the frequency of ω_r and a dc component in the transient components of the stator and rotor fault currents.

Table 1.The eigenvalues of the system matrix

R_c/R_r	eigenvalues	
	$p_{c1,2}$	$p_{c3,4}$
10	-8.39±j1.31	-66.88±j375.68
20	-7.85±j2.34	-128.08±j374.66
40	-6.30±j3.55	-250.82±j373.44
80	-3.79±j3.68	-495.79±j373.31
120	-2.57±j3.08	-739.47±j373.61
160	-1.99±j2.54	-982.52±j374.45

By increasing the crowbar resistance, τ_{Acs} increases and τ_{Acr} decreases. It means that by increasing the crowbar resistance, the damping speed of the dc component in the stator fault current decreases and the damping speed of the ac component with the frequency of ω_r increases. Moreover, the damping speed of the ac component with frequency of ω_r is much larger than that of the dc component.

Since the eigenvalues of matrix $\boldsymbol{A}_c$ are affected by the crowbar resistance, and the coupling between the stator flux linkage and rotor flux linkage cannot be neglected, the analysis of the stator flux linkage after the crowbar protection is activated is very complicated. Hence, it is necessary to establish a simplified calculation model of the stator flux linkage.

3.2 A Simplified calculation model of the DFIG stator flux linkage

In order to analyze the DFIG stator flux linkage under any kind of fault states (including the asymmetric and symmetric faults), the DFIG stator voltage during a grid fault can be expressed as

$$\begin{cases} u_{sa} = U_{sa}\sin(\omega_1 t + \alpha_1) \\ u_{sb} = U_{sb}\sin(\omega_1 t + \alpha_2) \\ u_{sc} = U_{sc}\sin(\omega_1 t + \alpha_3) \end{cases} \tag{12}$$

As noted, there are no special requirements on the amplitudes and phase angles of the three-phase voltages. Hence, (12) is the universal expression of the stator voltage that can be applied to any kind of the fault states.

Performing coordinate transformation to (12), the stator voltage under the $\alpha\beta$ reference frame is given by

$$\begin{cases} u_{s\alpha} = U_{s\alpha}\sin(\omega_1 t + \theta_1) \\ u_{s\beta} = -U_{s\beta}\cos(\omega_1 t + \theta_2) \end{cases} \tag{13}$$

where:

$U_{s\alpha} = 2\sqrt{U_{s\alpha1}^2 + U_{s\alpha2}^2}/3$, $\theta_1 = \arctan(U_{s\alpha1}/U_{s\alpha2})$,

$U_{s\alpha1} = U_{sa}\sin\alpha_1 - U_{sb}\sin\alpha_2/2 - U_{sc}\sin\alpha_3/2$,

$U_{s\alpha2} = U_{sa}\cos\alpha_1 - U_{sb}\cos\alpha_2/2 - U_{sc}\cos\alpha_3/2$,

$U_{s\beta} = \sqrt{3(U_{s\beta1}^2 + U_{s\beta2}^2)}/3$, $\theta_2 = \arctan(U_{s\beta1}/U_{s\beta2})$,

$U_{s\beta1} = U_{sb}\cos\alpha_2 - U_{sc}\cos\alpha_3$,

$U_{s\beta2} = U_{sc}\sin\alpha_3 - U_{sb}\sin\alpha_2$.

Though the equivalent resistance of the rotor windings is large at activation of the crowbar protection, the stator resistance is still very small and can be neglected.

By substituting (13) to (3), the expressions of the stator flux linkage with no consideration of damping are given by

$$\begin{cases} \psi_{s\alpha}(t) = \psi_{s\alpha0} + \dfrac{U_{s\alpha}}{\omega_1}\cos\theta_1 - \dfrac{U_{s\alpha}}{\omega_1}\cos(\omega_1 t + \theta_1) \\ \psi_{s\beta}(t) = \psi_{s\beta0} + \dfrac{U_{s\beta}}{\omega_1}\sin\theta_2 - \dfrac{U_{s\beta}}{\omega_1}\sin(\omega_1 t + \theta_2) \end{cases} \tag{14}$$

Actually, the dc components in the stator flux linkage always decay with time due to the stator resistance. With consideration of damping, the expressions of the stator flux linkage can be rewritten as

$$\begin{cases} \psi_{s\alpha}(t) = \left(\psi_{s\alpha0} + \dfrac{U_{s\alpha}}{\omega_1}\cos\theta_1\right)e^{-t/\tau_s} - \dfrac{U_{s\alpha}}{\omega_1}\cos(\omega_1 t + \theta_1) \\ \psi_{s\beta}(t) = \left(\psi_{s\beta0} + \dfrac{U_{s\beta}}{\omega_1}\sin\theta_2\right)e^{-t/\tau_s} - \dfrac{U_{s\beta}}{\omega_1}\sin(\omega_1 t + \theta_2) \end{cases} \tag{15}$$

In [9-11], it is assumed that the damping-time constant in (15) is the same as the equivalent-time constant of the stator windings, i.e. $\tau_s = L_t/(L_r R_s)$. However, as stated in the previous sub-section, the dynamic characteristics of the stator flux linkage are very complicated after the crowbar protection is activated. Using the handling method for the damping-time constant given in [9-11] would result in a large error. Assuming $\tau_s = L_t/(L_r R_s)$, Fig. 1 shows a comparison between the simulation and theoretical results of the stator flux linkage at a symmetric voltage dip.

As shown in Fig. 1, using the handling method that makes the damping-time constant in (15) equal to the equivalent-time constant of stator windings would result in a larger error. Hence, employing the above handling method to calculate the damping time constant is not reasonable.

Compromising between the accuracy and simplicity, τ_{Acs} is adopted as the damping-time constant of the transient components of the stator flux linkage. Fig. 2 demonstrates a comparison between the simulation result and the corresponding theoretical result of the stator flux linkage.

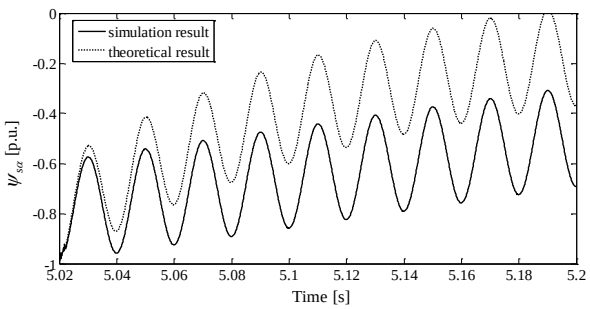

Fig. 1 Stator winding flux for a conventional simplification

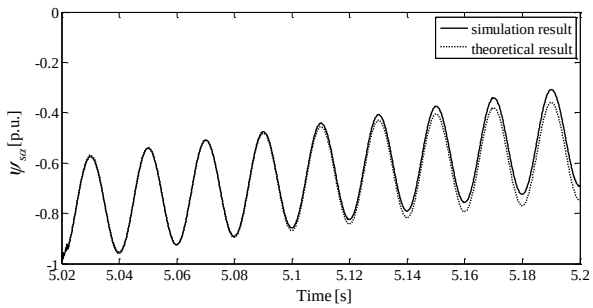

Fig. 2 Stator winding flux for the proposed simplification

As shown in Fig. 2, due to the impact of the coupling between the stator flux linkage and rotor flux linkage, the dynamic characteristics of the stator flux linkage are very complicated and cannot be simply described by (15). However, using the handling method that equals damping-time constant in (15) with τ_{Acs} can assure a high accuracy in the first four cycles. It means that it is reasonable to employ the proposed handling method for the damping-time constant in the first four cycles. Moreover, the proposed handling method is of great significance for the calculation of the maximum value

of the fault current and performance evaluation of a fast relaying protection.

Furthermore, though introduction of the crowbar resistance makes the dynamic characteristics of the stator flux linkage very complicated, the steady-state features of the stator flux linkage are not affected by the crowbar resistance. It means that the steady-state components expressed in (15) are accurate.

4 STUDY OF THE DFIG STATOR FAULT CURRENT

4.1 Characteristics analysis of the stator flux linkage

The following equations can be obtained according to (4).

$$\begin{cases} i_{r\alpha} = \psi_{s\alpha}/L_m - L_s i_{s\alpha}/L_m \\ i_{r\beta} = \psi_{s\beta}/L_m - L_s i_{s\beta}/L_m \end{cases} \tag{16}$$

$$\begin{cases} \psi_{r\alpha} = L_r\psi_{s\alpha}/L_m - L_t i_{s\alpha}/L_m \\ \psi_{r\beta} = L_r\psi_{s\beta}/L_m - L_t i_{s\beta}/L_m \end{cases} \tag{17}$$

After activation of the crowbar protection, the rotor voltage is zero, which means

$$u_{r\alpha} = 0,\ u_{r\beta} = 0 \tag{18}$$

Substituting (16), (17) and (18) to the last two equations in (3), the following equations are obtained:

$$\begin{cases} 0 = R_r'\psi_{s\alpha} + L_r\, d\psi_{s\alpha}/dt + \omega_r L_r \psi_{s\beta} \\ \quad - R_r' L_s i_{s\alpha} - L_t\, di_{s\alpha}/dt - \omega_r L_t i_{s\beta} \\ 0 = R_r'\psi_{s\beta} + L_r\, d\psi_{s\beta}/dt - \omega_r L_r \psi_{s\alpha} \\ \quad - R_r' L_s i_{s\beta} - L_t\, di_{s\beta}/dt + \omega_r L_t i_{s\alpha} \end{cases} \tag{19}$$

Consequently, the expressions of the stator current are given by

$$\begin{cases} i_{s\alpha}(t) = a_{\alpha 0} e^{-t/\tau_s} + e^{-t/\tau_r}\left(a_{\alpha 1}\sin\omega_r t + a_{\alpha 2}\cos\omega_r t\right) \\ \qquad + a_{\alpha 3}\sin\omega_1 t + a_{\alpha 4}\cos\omega_1 t \\ i_{s\beta}(t) = a_{\beta 0} e^{-t/\tau_s} + e^{-t/\tau_r}\left(a_{\beta 1}\sin\omega_r t + a_{\beta 2}\cos\omega_r t\right) \\ \qquad + a_{\beta 3}\sin\omega_1 t + a_{\beta 4}\cos\omega_1 t \end{cases} \tag{20}$$

where $\tau_r = L_r'/R_r'$, representing the equivalent damping-time constant of the rotor windings. The coefficients are given in Appendix B.

The three-phase stator currents can be obtained by performing coordinate transformation to (20).

As shown in Eq. (20), the dc components in the stator current maintain the stator flux linkage before and after activation of the crowbar protection. Likewise, in order to maintain the rotor flux linkage, there should be the dc components in the rotor current. In order to counteract the alternating flux linkage caused by the dc components in the rotor current, there are the ac components with the frequency of ω_r in the stator current, as shown in (20). Both the dc component and the ac component decay with time. Moreover, it can be seen that the ac damping component in the DFIG stator current is different from the damping component with the frequency of ω_1 in the stator current of the conventional synchronous generator.

The initial values of the dc and the ac components are related to the fault-occurrence time, the voltage amplitude after the fault occurrence and the DFIG rotor speed. Besides for the damped ac component with the frequency of ω_r and damped dc component, there is also a steady-state component with the frequency of ω_1 in the DFIG stator current. The amplitude of the steady-state component current is determined by the voltage amplitude after the fault occurrence and the DFIG rotor speed.

Though the steady-state components in the DFIG stator current are obtained with the simplified calculation model of the stator flux linkage, they are very accurate, since the steady-state components of the stator flux linkage expressed in (15) are accurate as well. It means that the steady-state components of the stator current expressed in (20) can accurately reflect the steady-state features of the stator current under real fault states.

4.2 Case study

In order to validate the above theoretical results, a DFIG simulation model is made in PSCAD/EMTDC. The DFIG parameters are given in Appendix A.

The three-phase and two-phase voltage dips are used to implement the simulation case studies. Several simulation cases under different voltage dip depth states are studied. However, considering the manuscript length, only the cases where voltages drop to 0.2 p.u. are illustrated in this paper. It is noted that DFIG is in its rated operating state and the rotor speed is 1.2 p.u. before the fault occurrence.

With the three-phase voltages all dropped to 0.2 p.u., Fig. 3 provides a comparison between the simulation and the theoretical results of the three-phase stator currents. With the voltages of phase B and phase C both dropped to 0.2 p.u., Fig. 4 shows a comparison between the simulation and the theoretical results of three-phase stator currents.

As shown in Figs. 3 and 4, the theoretical result of the stator fault current obtained with the proposed simplified calculation model of the stator flux linkage agrees with the simulation result very well in the first two cycles after the fault occurrence. After the transient components in the stator fault current decay completely, the waveform of the steady-state components of the stator current obtained according to (20) exactly match the simulation waveform. Hence, the above theoretical results are validated.

According to the requirements of the principle study and calculation of the relay protection, the maximum and the steady-state values of the fault current are very important parameters. As stated above, the accuracy of the analytical expressions of the DFIG stator current is

rather high in the first two cycles after the fault occurrence and during the steady-state period. Moreover, the maximum value of the fault current usually occurs in the first cycle after the fault occurrence. This means that the calculation results of the maximum and the steady-state values of the fault current obtained with the simplified calculation model of the stator flux linkage are accurate enough for the relay protection study. Hence, the analytical expressions of the DFIG stator current given in (20) meet the requirements of principle study and calculation of relay protection.

It should be noted that there are no approximation and assumption of the grid voltage made for the above theoretical analysis. Hence, the above theoretical analysis results can be applied for any kind of fault states.

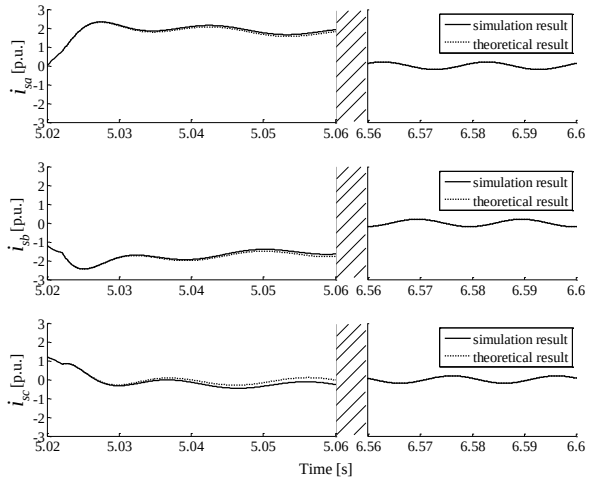

Fig. 3 Three-phase stator currents for the three-phase voltage dips

5 CONCLUSIONS

In order to meet the needs of the DFIG fault-current analysis under any kind of fault states, a DFIG dynamic model in the stator stationary reference frame is developed. Based on it, the dynamic characteristics of the stator flux linkage and characteristics of the stator fault current are studied. Finally, the analytical expressions of the stator current are obtained.

1) Since introduction of the crowbar resistance significantly increases the coupling between the stator and the rotor flux linkage, the dynamic characteristics of the stator flux linkage are very complicated. The stator flux linkage in the first four cycles after the fault occurrence and during the steady-state period can be studied accurately with the proposed calculation model.

2) Using the proposed calculation model of the stator flux linkage provides analytical expressions for the DFIG stator current under any kind of fault states. The simulation results show that the accuracy of the analytical expressions is rather high in the first two cycles after the fault occurrence and during the steady-state period, thus meeting the requirements of the principle study and calculation of relay protection.

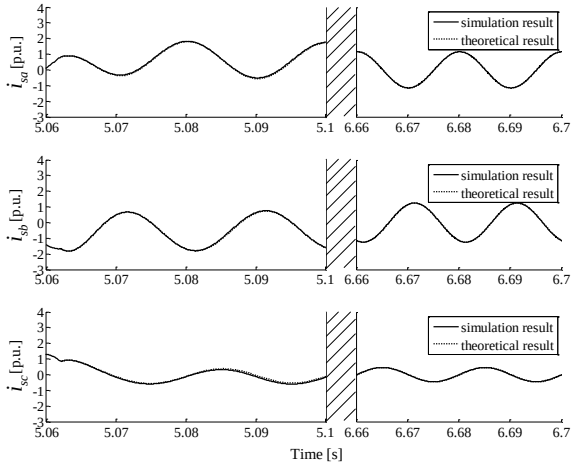

Fig. 4 Three-phase stator currents for the two-phase voltage dips

3) Besides for the steady-state component with the frequency of ω_1 and the damped dc component, there is also the damped ac component with the frequency of ω_r in the DFIG stator current. It means that the DFIG fault-current characteristics differ from those of the conventional synchronous generator.

The research results proposed in this paper are of great significance for setting an approximate relay protection system for the power grid with DFIG penetration.

ACKNOWLEDGEMENTS

This work was supported by the National Natural Science Foundation of China (Grant No. 51177058).

APPENDIX A

The parameters of DFIG are

Rated capacity: 1.5 MVA
Rated voltage: 690 V
Stator resistance (p.u.): 0.00756
Stator leakage reactance (p.u.): 0.1425
Rotor resistance (p.u.): 0.00533
Rotor leakage reactance (p.u.):0.1425
Mutual reactance (p.u.): 2.1767
Rated rotor speed (p.u.):1.2

APPENDIX B

Let $\tau_r = L_r'/R_r'$, $a = -1/\tau_r + 1/\tau_s$, $b = \omega_r - \omega_1$, $c = \omega_r + \omega_1$, $C_1 = \psi_{s\alpha 0} + \frac{U_{s\alpha}}{\omega_1}\cos\theta_1$, $C_2 = \frac{U_{s\alpha}}{\omega_1}$, $C_3 = \psi_{s\beta 0} + \frac{U_{s\beta}}{\omega_1}\sin\theta_2$, $C_4 = \frac{U_{s\beta}}{\omega_1}$, $C_5 = \frac{L_m^2 R_r'}{L_t^2}$, $C_6 = \frac{b}{b^2 + 1/\tau_r^2}$, $C_7 = \frac{c}{c^2 + 1/\tau_r^2}$, $C_8 = \frac{1/\tau_r}{b^2 + 1/\tau_r^2}$, $C_9 = \frac{1/\tau_r}{c^2 + 1/\tau_r^2}$.

The coefficients in (17) are respectively

$$a_{\alpha 0}=\frac{C_1}{L_s'}+C_1C_5\frac{a}{\omega_r^2+a^2}+C_3C_5\frac{\omega_r}{\omega_r^2+a^2}$$

$$\begin{aligned}a_{\alpha 1}=&-C_1C_5\frac{\omega_r}{\omega_r^2+a^2}+C_3C_5\frac{a}{\omega_r^2+a^2}-i_{s\beta 0}+\frac{\psi_{s\beta 0}}{L_s'}\\&+\frac{C_2C_5}{2}\sin\theta_1\left(C_8-C_9\right)+\frac{C_2C_5}{2}\cos\theta_1\left(C_6+C_7\right)\\&+\frac{C_4C_5}{2}\sin\theta_2\left(C_8+C_9\right)+\frac{C_4C_5}{2}\cos\theta_2\left(C_6-C_7\right)\end{aligned}$$

$$\begin{aligned}a_{\alpha 2}=&-C_1C_5\frac{a}{\omega_r^2+a^2}-\frac{C_2C_5}{2}\cos\theta_1\left(C_8+C_9\right)-\frac{\psi_{s\alpha 0}}{L_s'}\\&+\frac{C_2C_5}{2}\sin\theta_1\left(C_6-C_7\right)-C_3C_5\frac{\omega_r}{\omega_r^2+a^2}+i_{s\alpha 0}\\&+\frac{C_4C_5}{2}\sin\theta_2\left(C_6+C_7\right)-\frac{C_4C_5}{2}\cos\theta_2\left(C_8-C_9\right)\end{aligned}$$

$$\begin{aligned}a_{\alpha 3}=&\frac{C_2}{L_s'}\sin\theta_1-\frac{C_2C_5}{2}\cos\theta_1\left(C_6-C_7\right)\\&-\frac{C_2C_5}{2}\sin\theta_1\left(C_8+C_9\right)+\frac{C_4C_5}{2}\sin\theta_2\left(C_9-C_8\right)\\&-\frac{C_4C_5}{2}\cos\theta_2\left(C_6+C_7\right)\end{aligned}$$

$$\begin{aligned}a_{\alpha 4}=&-\frac{C_2}{L_s'}\cos\theta_1+\frac{C_2C_5}{2}\cos\theta_1\left(C_8+C_9\right)\\&+\frac{C_2C_5}{2}\sin\theta_1\left(C_7-C_6\right)-\frac{C_4C_5}{2}\sin\theta_2\left(C_6+C_7\right)\\&+\frac{C_4C_5}{2}\cos\theta_2\left(C_8-C_9\right)\end{aligned}$$

$$a_{\beta 0}=\frac{C_3}{L_s'}+C_3C_5\frac{a}{\omega_r^2+a^2}-C_1C_5\frac{\omega}{\omega_r^2+a^2}$$

$$a_{\beta 1}=a_{\alpha 2},\ a_{\beta 2}=-a_{\alpha 1}$$

$$\begin{aligned}a_{\beta 3}=&-\frac{C_4}{L_s'}\cos\theta_2-\frac{C_4C_5}{2}\sin\theta_2\left(C_6-C_7\right)\\&+\frac{C_4C_5}{2}\cos\theta_2\left(C_8+C_9\right)+\frac{C_2C_5}{2}\cos\theta_1\left(C_8-C_9\right)\\&-\frac{C_2C_5}{2}\sin\theta_1\left(C_6+C_7\right)\end{aligned}$$

$$\begin{aligned}a_{\beta 4}=&-\frac{C_4}{L_s'}\sin\theta_2+\frac{C_4C_5\sin\theta_2}{2}\left(C_8+C_9\right)\\&+\frac{C_4C_5\cos\theta_2}{2}\left(C_6-C_7\right)+\frac{C_2C_5}{2}\cos\theta_1\left(C_6+C_7\right)\\&+\frac{C_2C_5}{2}\sin\theta_1\left(C_8-C_9\right)\end{aligned}$$

where, $i_{s\alpha 0}$, $i_{s\beta 0}$, $\psi_{s\alpha 0}$ and $\psi_{s\beta 0}$ are respectively the initial values of stator current and stator flux linkage under $\alpha\beta$ reference frame when the fault occurs.

REFERENCES

[1] Q. Liu, Y. He, J. Zhang, Operation Control and modeling-simulation of AC-excited variable-speed constant-frequency wind power generator, Proceedings of the CSEE, vol. 26, no. 5, pp. 43-50, 2006.

[2] S. Muller, M. Deicke, R. W. De Doncker, Doubly fed induction generator systems for wind turbines, IEEE Industry Applications Magazine, vol. 8, no. 3, pp. 26-33, 2002.

[3] F. M. Hughes, O. A. Lara, N. Jenkins, G. Strbac, Control of DFIG-based wind generation for power network support, IEEE Transaction on Power Systems, vol. 20, no. 4, pp. 1958-1966, 2005.

[4] G. Pannell, D. J. Atkinson, B. Zahawi, Minimum-threshold crowbar for a fault-ride-through grid-code-compliant DFIG wind turbine, IEEE Transaction on Energy Conversion, vol. 25, no. 3, pp. 750-759, 2010.

[5] D. Xie, Z. Xu, L Yang., J. Ostergaard, Y. Xue, W. P. Kit, A comprehensive LVRT control strategy for DFIG wind turbines with enhanced reactive power support, IEEE Transaction on Power Systems, vol. 28, no. 3, pp. 3302-3310, 2013.

[6] M. Tsili, S. Papathanassiou, A review of grid code technical requirements for wind farms, IET Renewable Power Generation, vol. 3, no. 3, pp, 308-322, 2009.

[7] J. Morren,S. W. H. de Haan, Ridethrough of wind turbines with doubly-fed induction generator during a voltage dip, IEEE Transaction on Energy Conversion, vol. 2, no. 1, pp. 435-441, 2005.

[8] A. Han, Z. Zhang, X. Yin, J. Zhang, M. Liang, Research on fault characteristic and grid connecting-point protection scheme for wind power generation with doubly-fed induction generator, Transactions of China Electrotechnical Society, vol. 27, no. 4, pp. 233-239, 2012.

[9] H. Zhou, G. Yang, Short circuit current characteristics of doubly fed induction generator with crowbar protection under different voltage dips, Proceedings of the CSEE, vol. 29, no. S1, pp. 184-191, 2009.

[10] M. S. Vicatos, J. A. Tegopoulos, Transient state analysis of a doubly-fed induction generator under three phase short circuit, IEEE Transactions on Energy Conversion, vol. 6, no. 1, pp. 62-68, 1991.

[11] J. Morren, S. W. H. de Haan, Short-circuit current of wind turbines with doubly-fed induction generator, IEEE Transactions on Energy Conversion, vol. 22, no. 1, pp. 174-180, 2007.

[12] J. Zhai, B. Zhang, G. Xie, C. Mao, K. Wang, Three-phase symmetrical short-circuit current characteristics analysis of wind turbine driven DFIG with crowbar protection, Automation of Electric Power Systems, vol. 37, no. 3, pp. 18-23, 2013.

[13] J. Zhang, X. Chen, H. Liu, P. Wang, B. Wang, There-phase short-circuit analysis for double-fed wind-driven generator and short-circuit maximal resistance calculation, Electric Power Automation Equipment, vol. 29, no. 4, pp. 6-10, 2009.

[14] L. Xu, Coordinated control of DFIG's rotor and grid side converters during network unbalance, IEEE Transactions on Power Electronics, vol. 22, no. 3, pp. 1041-1049, 2008.

Xiangping Kong is currently working towards his Ph.D. degree at Huazhong University of Science and Technology (HUST), Wuhan, China.
His research interest is in protection of the power grid with penetration of distributed generators.

Zhe Zhang received his Ph.D. degree in electrical engineering from HUST, Wuhan, China, in 1992.
Currently, he is a professor at the School of Electrical and Electronic Engineering, HUST. His interest is in protective relaying.